

Analysis of Synthetic Inertia Strategies from Wind Turbines for Large System Stability

Alberto Berizzi , Member, IEEE, Alessandro Bosisio , Valentin Ilea , Danilo Marchesini, Roberto Perini , Member, IEEE, and Andrea Vicario 

Abstract—In this article, two different strategies to enhance power system stability exploiting synthetic inertia are presented and compared to assess the possibility of increasing the penetration of converter-based generation in power systems, keeping a suitable stability margin. Synthetic inertia is the emulation, carried out by converted-based generation, of the inertial response provided by rotating generators during frequency events. Two approaches are hence described, focusing on wind power. In the first approach, the primary power source is connected to the grid by a grid-following converter, and it exploits the energy content of the direct current link, suitably sized (or, with the same concept, of a suitable energy buffer available). The second approach uses a grid-forming converter model, whose features resemble more a traditional synchronous machine. The article aims at assessing the contribution to frequency stability that can be provided by converter-based generation. The simulation results demonstrate that converter-based generation can efficiently guarantee frequency stability, thus proving that future power systems will be able to manage ever-increasing renewable energy source converter-based generation.

Index Terms—Grid-following, grid-forming, power system stability, synthetic inertia, wind energy integration.

I. INTRODUCTION

THE growing deployment of renewable energy sources (RESs) significantly affects the control and management of modern electric power systems. Nowadays, RES plants represent an increasing share of the total generation. However, they are raising stability and control issues since they are usually interfaced by electronic converters, not designed to support the system. In this perspective, a significant concern is generally associated with the decreasing amount of physical inertia (synchronous machines) directly connected to the system. Different countermeasures are available in the literature to control converters in such a way as to emulate physical inertia. Focusing mainly

Manuscript received June 20, 2021; revised September 13, 2021, November 29, 2021, and January 10, 2022; accepted February 20, 2022. Date of publication February 25, 2022; date of current version May 20, 2022. Paper 2021-PSEC-0490.R3, presented at 2020 IEEE International Conference on Environment and Electrical Engineering and 2020 IEEE Industrial and Commercial Power Systems Europe, Madrid, Spain, Jun. 9–12, and approved for publication in the IEEE TRANSACTIONS ON INDUSTRY APPLICATIONS by the Power Systems Engineering Committee of the IEEE Industry Applications Society. (Corresponding author: Andrea Vicario.)

The authors are with the Department of Energy, Politecnico di Milano, 20156 Milano, Italy (e-mail: alberto.berizzi@polimi.it; alessandro.bosisio@polimi.it; valentin.ilea@polimi.it; danilo.marchesini@polimi.mail.it; roberto.perini@polimi.it; andrea.vicario@polimi.it).

Color versions of one or more figures in this article are available at <https://doi.org/10.1109/TIA.2022.3154671>.

Digital Object Identifier 10.1109/TIA.2022.3154671

on wind power, but not limiting to it, in [1], the inertia response is emulated, exploiting the energy content of the direct current (DC) link of a fully rated converter (FRC). That methodology is validated in this article and compared to other approaches.

Similarly, a doubly fed induction generator (DFIG) is considered in [2] and [3] to provide inertia emulation, while in [4], the rotating mass connected to the DFIG shaft and a supercapacitor connected via a dc/dc converter to a back-to-back inverter are used for the same goal. In [5], fast frequency response is provided by wind turbines, recovering the rotor speeds in a longer time scale, i.e., during the secondary frequency control action. Finally, in [6], an active power droop control is proposed to control power converters in alternating current (AC) microgrids. A comprehensive literature review on control types for providing inertia can be found in [7]. It is worth noticing that the above-mentioned papers focus on the converter control, but do not provide an assessment of their contribution to the stability of a real, large power system. One of the goals of this article is also to fill this gap, thus showing the way for decarbonized future power systems.

According to ENTSO-E, the European Network of Transmission System Operators for Electricity, synthetic inertia emulation is defined as “*the facility provided by a power park module or HVDC system to replace the effect of the inertia of a synchronous power-generating*” [8]. Therefore, synthetic inertia corresponds to the controlled action of an inverter-based generating unit to mimic the exchange of kinetic energy of a rotating generator to the power system. As RESs are going to replace conventional generators, inertia is expected to be reduced, leading to an increasing rate of change of frequency (RoCoF) in the case of transients [7], unless it is replaced somehow from converters.

A variety of definitions exists in the literature to identify different converter control strategies [6] are as follows.

- 1) *Grid-Following Power Converters*: They can be modelled as controlled current sources with a high parallel output impedance that inject real and reactive power according to a defined power or current setpoint. They are best operated when a stable voltage reference (infinite system) is available.
- 2) *Grid-Forming Power Converters*: They can be modeled as closed-loop controlled voltage sources with low output impedance. The controller, usually defined by a droop control function or similar approaches [9], [10], needs the reference voltage and frequency as inputs.

Different mechanisms are proposed to link the frequency variation to the converter power injection for grid-following converters. In [1], the implementation of the synthetic inertia is obtained acting on the control of a back-to-back inverter associated with a wind power plant. Some authors introduced either a proportional [11], or even “square-root” [12], dependency of the dc voltage reference as a function of the frequency deviation from its nominal value. Nevertheless, these latter approaches do not always guarantee the convergence of dc voltage to its nominal value when the transient has expired. Another possible architecture mimics the inertial effect from battery storage systems as a transient power injection proportional to the frequency derivative [13].

On the other side, the initial, main idea behind the grid-forming concept was to provide a voltage reference, thus enabling the operation of other grid-following converters in islanded systems. However, grid-forming converters can also facilitate the integration of multiple distributed generators in existing bulk power systems, as they can enhance frequency stability thanks to their intrinsic ability to emulate synchronous generators. Researchers have investigated this capability, as reported in [9], where grid-forming converters are compared to the grid-following approach, or in [10], where the interaction between grid-forming inverters and the bulk power system is investigated. Finally, [14] examines the interaction of grid-forming converters with the dynamics of the synchronous machines.

The innovative content of the article is twofold: on one side, it presents a design procedure for FRC-based wind power converters set-up according to [1] to make it possible for grid-following converter-based generation (currently, the most widespread in power systems) to contribute to power system stability by providing an inertial response to face system perturbations. On the other side, the impact of wide implementation of synthetic inertia mechanisms on many converters in the grid is evaluated from the power system stability point of view to assess the viability of a “nearly 100% RES converter-based” generation. To this aim, results from a lab test facility and simulations to compare the presented approach to other control techniques proposed in the literature [applied to grid-following/grid-forming converters, wind power based on FRC/DFIG, battery energy storage systems (BESS)] are shown, with reference to large power system angle and frequency stability. While the article mainly refers to wind power, the same conclusions are also valid for photovoltaic (PV) generation connected to the power systems.

Comparisons are carried out on different case studies: first, the grid-following control strategy is presented and explained on a simple high voltage (HV) network; then, to evaluate the impact on a large power system, a comparison with different strategies from the recent technical literature to provide inertia is carried out by means of simulations on both an IEEE test system and a large portion of the real Italian transmission system, namely Sicily.

The article is organized as follows: the control strategy for the grid-following design procedure is presented in Section II. The grid-forming control is described in Section III; Section IV presents all performances and comparisons on the three considered power systems. Finally, conclusion is provided in Section V.

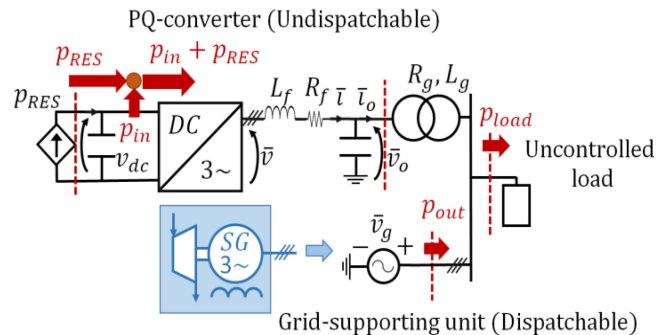


Fig. 1. Electrical scheme for synthetic inertia analysis in isolated microgrids.

II. GRID-FOLLOWING WITH INERTIA EMULATION

The first control strategy is related to the grid-following converters. It proposes a way to emulate the inertial response provided by traditional generators, supplying a temporary contribution during the first instants of a transient. This contribution requires a change in the power through the converter. While it is not an issue for a suitably sized storage system, it may be a problem when the converter connects the grid to a wind or PV plant, tracking the maximum power available. In this case, it is necessary to exploit either the acceleration or deceleration of rotating masses (in the case of a wind turbine or a flywheel) or the energy stored in the capacitor installed on the dc link of the dc/ac converter. The advantage of this latter solution is demonstrated to be twofold: first, the inertial response can be provided by any types of plants connected by converters, either a wind turbine or a PV plant with or without an associated storage system, assuming that a sufficient energy buffer is installed. Second, focusing on wind generators, problems associated with the use of physical inertia, which could potentially lead to rotor instability, are avoided [2]. Among the different wind power drive trains, wind generators type 4 (FRC) are employed because: they currently hold the largest share of the new installations and they can also model connection of PV or BESS plants.

In a generic system, where all parameters are well known and constant with time (e.g., a small system or a microgrid, Fig. 1), the main issue is typically evaluating stability limits associated with the interactions between dispatchable generators and nondispatchable RES units.

The transfer function between the load power p_{load} and the grid angular frequency ω_g , which influences the stability of the system, can be found from a power balance (see Fig. 1)

$$p_{\text{RES}} + p_{\text{in}} + p_{\text{out}} - p_{\text{load}} = 0 \quad (1)$$

$$\Delta p_{\text{RES}} + \Delta p_{\text{in}} + \Delta p_{\text{out}} - \Delta p_{\text{load}} = 0 \quad (2)$$

where p_{RES} is the power delivered by the RES source, which is assumed constant

$$\Delta p_{\text{RES}} = 0 \quad (3)$$

where p_{in} is the contribution to the synthetic inertia of the not dispatchable unit, whose variation is

$$\Delta p_{\text{in}} = -s K_{\text{in}} \Delta \omega_g \quad (4)$$

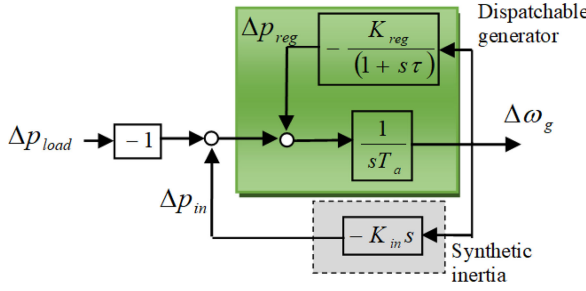


Fig. 2. Microgrid regulation model, under synthetic inertia control.

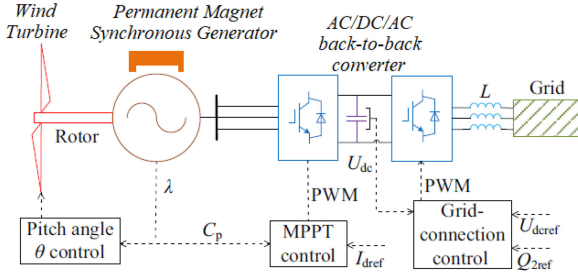


Fig. 3. Back-to-back converters of a wind turbine [16].

where p_{out} is the power delivered by the dispatchable unit, made up of a primary frequency regulation power p_{reg} , and the inertial one $p_{inertial}$, whose variation is

$$\Delta p_{out} = \Delta p_{reg} + \Delta p_{inertial} = -\frac{K_{reg}}{1+s\tau} \Delta\omega_g - sT_a \Delta\omega_g \quad (5)$$

where K_{reg} is the droop coefficient, τ the delay, while T_a is the starting time of the unit.

The previous equations can be represented through a block diagram (see Fig. 2) which highlights the relation between the load power and the grid frequency

$$\frac{\Delta\omega_g}{\Delta p_{load}} = -\frac{1+s\tau}{(T_a + K_{in}) \tau s^2 + (T_a + K_{in}) s + K_{reg}}. \quad (6)$$

The poles of this transfer function are heavily influenced by the gain K_{in} of the synthetic inertia. In fact, by assuming $\tau \ll T_a$, holds

$$p_1 \approx -\frac{1}{\tau}, \quad p_2 \approx -\frac{K_{reg}}{(T_a + K_{in})}. \quad (7)$$

Some disadvantages can be envisaged in this approach, which prevents its application to large-scale systems:

- 1) The parameters of both the dispatchable (T_a, K_{reg}, τ) and nondispatchable (R_g, L_g) generators are required for the stability analysis;
- 2) The linearized feedback model holds for small variations, neglecting saturations.

Numerical approaches are usually preferred in bulk power systems and are also adopted in this article. As depicted in Fig. 3, power electronics are made up of an ac/dc/ac back-to-back power converter. The generator-side converter is controlled to maintain the turbine in maximum power point tracking (MPPT) conditions. In contrast, the grid-side converter acts on the real

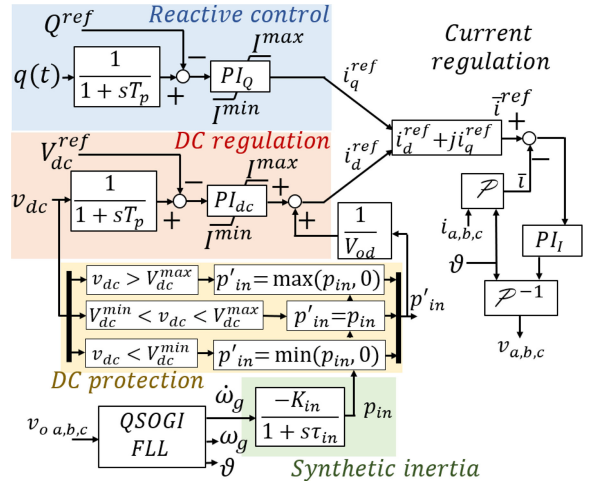


Fig. 4. Current-controlled model to enable synthetic inertia allowing dc voltage variation. This control structure refers to the grid-side converter of the back-to-back architecture, where P represents the Park transform [15].

power injected into the grid to keep the DC link voltage close to its nominal conditions. Additionally, reactive support to the network can be provided.

Fig. 4 depicts the control diagram of the system. A typical synchronous-frame structure is considered, and linear PI regulators, suitably equipped with saturation, are introduced. Two independent controllers are respectively associated with the dc bus stabilization and reactive injection; they provide separate direct i_d^{ref} and quadrature i_q^{ref} references for the internal current loop.

To implement synthetic inertia, the two major modes to vary the dc-bus voltage are: current-controlled (C.C.) mode and voltage-controlled (V.C.) mode [13]–[15]. In the C.C. mode, as also adopted in this article, the inertial control consists of an additional signal p_{in} introduced on the direct-axis reference, proportional to the frequency approximate derivative by the inertia coefficient K_{in} . Furthermore, its negative sign increases real power injection during under-frequency events by discharging the dc capacitor.

Supercapacitors or ultracapacitors give the possibility of oversizing the dc link. Their employment is not a novelty in wind power generation since they are employed for emergency pitch control or to compensate wind fluctuations. Lithium-ion supercapacitors present one of the highest power densities and can be employed for this purpose.

The dc voltage must be kept temporarily free to allow an inertial response of the power converter, thus enabling the charging or discharging of the capacitor in response to the system frequency disturbance without affecting the turbine operation. In order to extract the angular frequency derivative $\dot{\omega}_g$, the quadrature second-order generalized integrator - frequency locked loop (QSOGI-FLL) algorithm is adopted [17]. An additional filtering effect can be introduced combining the frequency-locked loop

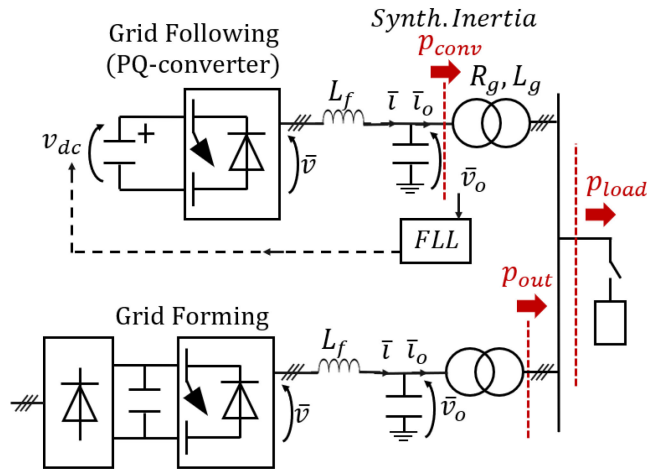


Fig. 5. Experimental set-up used for the testing.

(FLL) dynamics with a first-order low-pass filter with time-constant τ_{in} , modifying the inertia function as

$$p_{in} = -\frac{K_{in}}{1 + s \tau_{in}} \dot{\omega}_g. \quad (8)$$

The QSOGI-FLL method is also exploited to determine the Park transform synchronization angle associated with the rotating-axes control, as depicted in Fig. 4.

Differently from the procedure in [13]–[15], an additional block, called “dc protection,” has been introduced to decouple the design of the inertia coefficient K_{in} from the network characteristics. Moreover, this block guarantees the maximum exploitation of the available energy reserve and fulfills the technical/security constraints associated with the converters. Assuming a variability range $\Delta \dot{V}_{DC} = 0.1$ p.u., the sizing of the capacitance is given as

$$C_{DC} = \frac{10\% A_b \Delta t}{\frac{1}{2} (V_{DC \text{ nom.}}^2 - V_{DC \text{ min.}}^2)} \quad (9)$$

where A_b is the nominal design power of the equivalent wind generator exploited to model the renewable production plant, and Δt is the expected time duration of the frequency transient. The synthetic inertia is activated only when the discharge process is compatible with the dc voltage ratings; hence, when the dc voltage is lower than the minimum allowed value, discharge is inhibited, and only charging operations are allowed. Dually, discharging signals are the only ones sent to the control whenever the voltage is close to its maximum. This behavior can be identified considering the definition of the actual inertia signal p'_in in Fig. 4. Thanks to the introduction of the dc protection block, the accurate sizing of the inertia parameter is no longer fundamental: whatever the value of the K_{in} , when the lower voltage limit is reached, the synthetic inertia provision is stopped.

To select the best control to be adopted for subsequent time-domain simulations on large systems, a comparison has been carried out between the C.C. mode and V.C. mode available in the literature [13]–[15]. Some experimental tests have been carried out on a small-case lab facility (see Fig. 5): it consists of a grid-forming inverter (2.4 kVA, 200 V), supplied by the grid

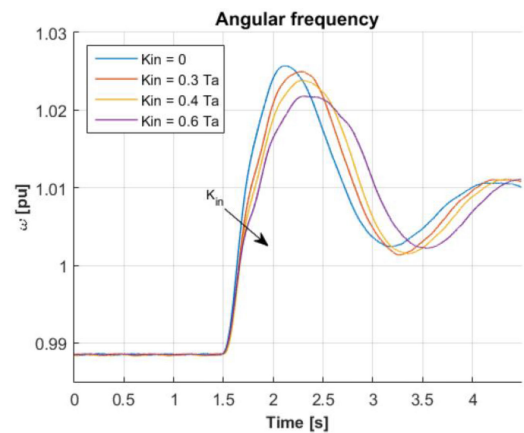


Fig. 6. Angular frequency profile for different values of the synthetic inertia K_{in} following a load disconnection, in C.C. mode.

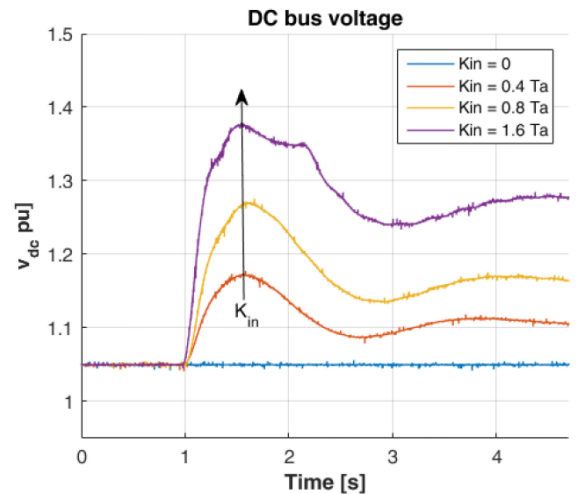


Fig. 7. DC-bus voltage profile for different values of the synthetic inertia K_{in} following a load disconnection, in V.C. mode. The voltage does not return to its nominal value.

through a diode bridge, and a grid-following inverter, whose dc-side is connected to a 8 mF capacitor. The perturbation Δp_{load} is generated by the control of the grid-forming inverter, emulating a dispatchable unit with starting time T_a (10 s) and delay time τ (0.5 s).

As for the C.C. strategy, Fig. 6 shows the grid angular frequency ω_g following a load disconnection $\Delta p_{load} = 1.0$ p.u.; it is worth noticing that a smoother variation can be obtained by increasing the synthetic inertia coefficient K_{in} from 0 to 0.6 T_a .

A second test (see Fig. 7) has been carried out adopting the V.C. strategy, where a synthetic inertial signal is added to the V_{DC}^{Ref} signal (see Fig. 4). While the frequency response gives results comparable to the C.C. strategy, it is worth observing that the dc-bus voltage does not go back to the nominal value at steady-state. This is why the C.C control was chosen for the implementation proposed in the article.

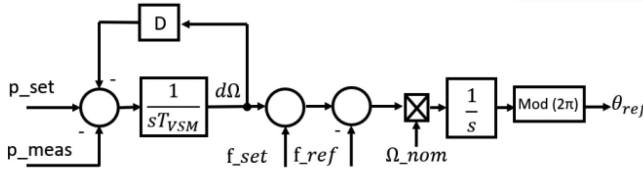


Fig. 8. Simplified control scheme of the VSM.

III. GRID-FORMING CONTROL STRATEGY

In this section, the control of the grid-forming converter adopted for comparison is presented. Among the different grid-forming control logics available, the most common are droop control [18] and virtual synchronous machine (VSM) [19], [20]. This article uses the VSM configuration of the DigSilent PowerFactory 2021 library, where the variables have been properly tuned for this comparison, and only a short recap is given here.

The main idea of the VSM grid-forming control strategy is to mimic the equation that describes the dynamics of a synchronous machine in a voltage source converter [19]

$$sT_{VSM} \cdot \omega_{VSM} \approx P_{set} - P_{meas} - D(\omega_{VSM} - \omega_g) \quad (10)$$

where $T_{VSM} = 2H$ is the mechanical time constant, twice the inertia constant to be emulated, P_{set} is the active power reference, P_{meas} is the measured electric power generated by the converter, and D is the damping coefficient. ω_{VSM} is the angular frequency setpoint for the machine and ω_g the grid angular frequency. In this way, it is possible to draw the block diagram of the desired control in DigSilent, as shown in Fig. 8. f_{set} is the setpoint frequency provided by a secondary controller, f_{ref} the reference frequency in RMS simulations (stability analysis functions), θ_{ref} is the voltage angle sent to the output voltage calculation, and finally to the static generator, controlled as a voltage source.

IV. RESULTS

This section presents a comprehensive comparison of the performances provided by the proposed synthetic inertia model for grid-following converters (grid-following FRC), to other devices and controls available in the technical literature, namely DFIG wind generators, BESS with virtual inertia provision and grid-forming converters. The results presented first are related to simulations carried out on a small test system to make it easy to understand the main features of the proposed control; then, the IEEE 14-bus system is used to provide a quantitative comparison to selected methods available in the existing literature. Finally, the Sicilian system, interconnected to the ENTSO-E European power system, has been used to evaluate the large-scale impact of the connection of a large number of converters equipped with a synthetic inertia control, thus assessing the feasibility of a nearly 100% RES converter-based generation. All tests have been performed using the RMS simulation function of DigSilent PowerFactory 2021, with an integration step size of 0.01 s, using an Intel Core i7-9750H CPU @ 2.60 GHz.

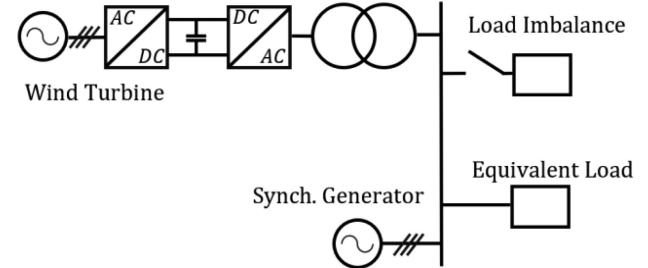


Fig. 9. Equivalent circuit of the small-scale HV isolated network used as the study case.

TABLE I
FULL-RATED CONVERTER WIND GEN

Parameter	Symbol	Value
Wind farm design power	A_b	45 MVA
DC bus capacitance	C_{dc}	2 F
DC nominal voltage	$V_{DC\ nom.}$	7.26 kV
Expected duration	Δt	2 s
Synth. inertia coefficient	K_{in}	8 s
Synth. inertia time const.	τ_{in}	0.1 s
Current loops cut-off freq.	ω_{CI}	$2\pi \cdot 350$ rad/s
Voltage loops cut-off freq.	ω_{CV}	$2\pi \cdot 1$ rad/s
FLL cut-off freq.	ω_{FLL}	100 rad/s

TABLE II
SMALL-SCALE TEST NETWORK

Parameter	Symbol	Value
Synch. generator size	A_{gen}	500 MVA
Synch. gen. droop	K_{reg}	0.04
Synch. gen. acceleration time constant	T_a	10 s
Network voltage level	V_{HV}	110 kV
Wind gen. nominal size	A_b	45 MVA
Wind gen. actual production	P_{wind}	15 MW
Load imbalance	ΔP_{load}	$0.1 \cdot P_{wind}$

A. Simulation on a Small-Scale Test System

The first test system considered is shown in Fig. 9, where an equivalent wind farm, represented by a single wind turbine, is connected to a large-scale synchronous generator and two loads. The parameters of the equivalent wind-farm control scheme of Fig. 4 are given in Table I.

The synchronous generator is equipped with a primary frequency regulation governor, and its characteristics are given in Table II. The perturbation simulated is a load connection, equal to 10% of the wind turbine production.

A first comparison (see Fig. 10) can be carried out between the case without any frequency support provided by the wind turbine (blue line) and the case with the contribution (red line).

Fig. 10 shows a significant improvement in the frequency nadir, both in amplitude and delay; additionally, the RoCoF is reduced when synthetic inertia is enabled. This result is significant

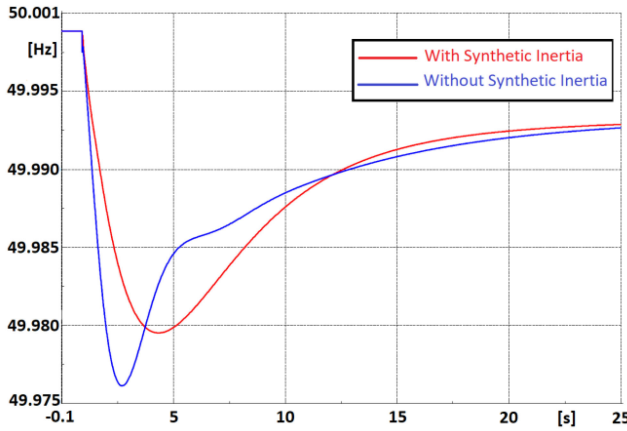


Fig. 10. Comparison between the frequency transients with and without synthetic inertia ($\Delta P_{\text{load}} = 10\%P_{\text{wind}}$).

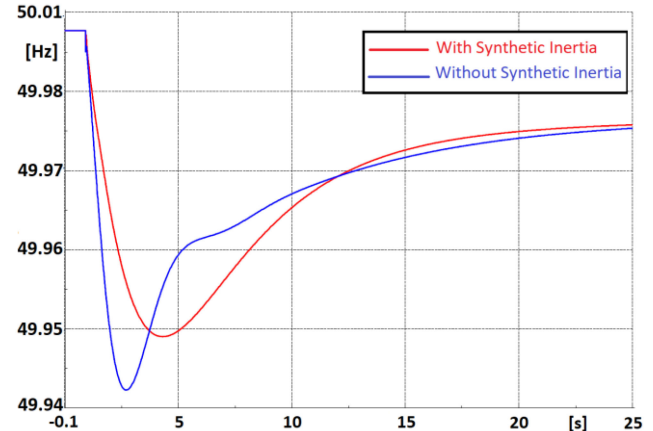


Fig. 12. Comparison between the frequency transients with and without synthetic inertia ($\Delta P_{\text{load}} = 30\%P_{\text{wind}}$).

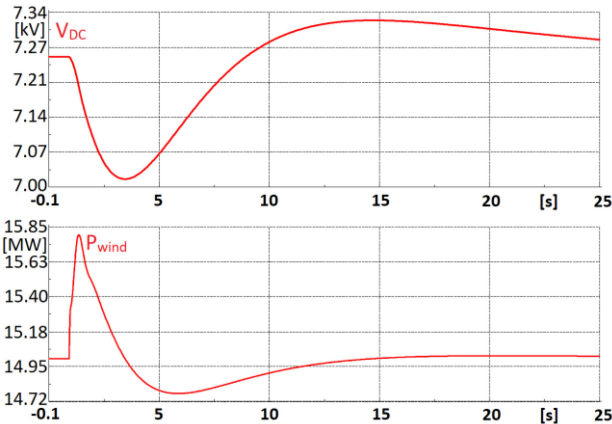


Fig. 11. DC voltage profile and active power output of the wind turbine generator at the point of connection ($\Delta P_{\text{load}} = 10\%P_{\text{wind}}$).

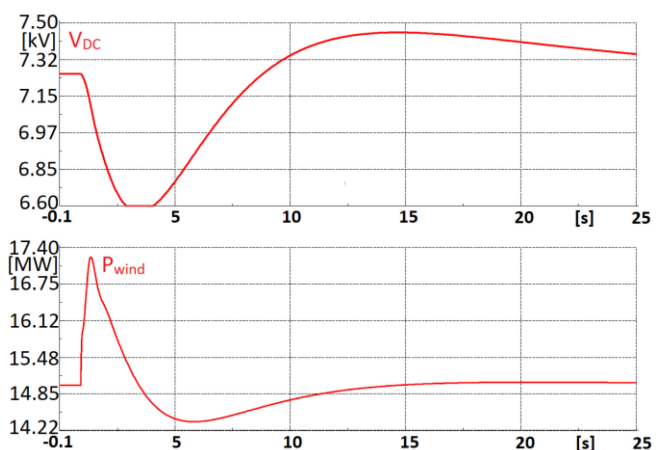


Fig. 13. DC voltage profile and active power output of the wind turbine generator at the point of connection ($\Delta P_{\text{load}} = 30\%P_{\text{wind}}$).

since, in real power systems, many Special protection schemes activate load shedding based on the frequency and/or RoCoF. The difference between the two curves becomes appreciable approximately after 250 ms, which is the equivalent delay related to the internal controllers.

Fig. 11 shows the dc voltage profile and the real power output of the wind plant. Initially, the dc voltage decreases to release the energy stored in the capacitor. Later on, the dc regulator brings back the dc voltage to its nominal value in less than 1 min. Finally, at the point of connection with the HV grid, the real power of the wind power plant is temporarily increased thanks to the discharge of the dc capacitor.

Figs. 12 and 13 show the grid and converter behavior under a more severe network unbalance, a load step of 30% of the wind production. In terms of the frequency transient, Fig. 12, the simulation confirms that the proposed synthetic inertia technique is effective in frequency nadir containment and reduces the average RoCoF. Fig. 13 shows that the dc voltage profile reaches its minimum limit (6.6 kV) the synthetic inertia support is inhibited by the scheme illustrated in Fig. 4: this allows providing the maximum available regulating energy without jeopardizing the stability of the converter.

Some sensitivity tests have been carried out to check the robustness of results to the features of the power system, described by the starting time of the equivalent generator. A load connection, equal to 10% of the wind turbine production, has been used to generate the frequency transient. In Fig. 14, the starting time constant of the equivalent synchronous generator has been reduced to $T_a = 5$ s, to simulate a lower inertia grid, keeping the same controller parameters. The benefit of the proposed control is significant: while the base case shows an oscillatory behavior, the introduction of the synthetic inertia control results in a nonoscillating smooth response, with lower nadir and RoCoF.

On the contrary, increasing $T_a = 20$ s gives the results depicted in Fig. 15, showing that a higher-inertia system is less affected by the same power imbalance, resulting in a lower initial RoCoF and a lower frequency nadir. Thus, in this case, the synthetic inertia improvement is less significant.

Finally, it is worth noticing that wind farms are typically made by several generators; hence, it is important to assess possible negative interactions among several plant controllers. Many simulations were carried out, checking that one equivalent generator

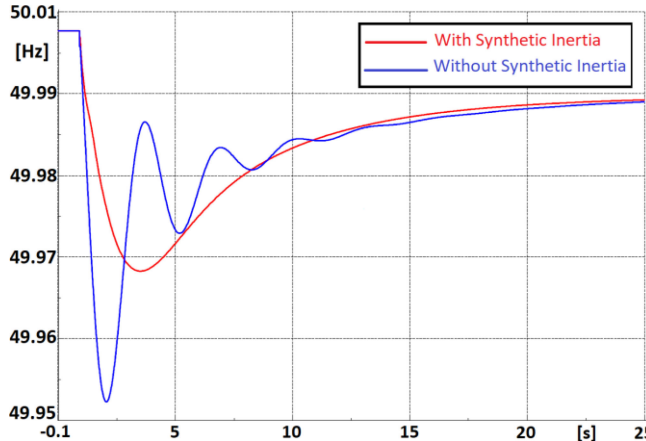


Fig. 14. Frequency behavior with and without synthetic inertia considering a low-inertia equivalent system ($T_a = 5$ s).

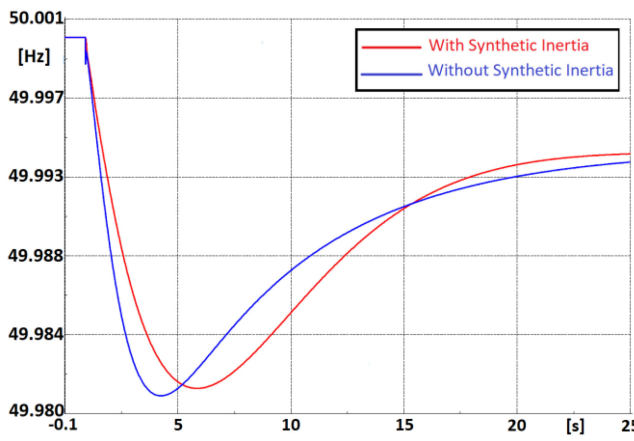


Fig. 15. Frequency behavior with and without synthetic inertia considering a high-inertia equivalent system ($T_a = 20$ s).

could provide the same results as ten and equal independent generators of 1.5 MVA, with their converters, as considered with the simplified network of Fig. 9. Such tests gave identical results, proving that an equivalent-single wind turbine can be used in more detailed grids with the same accuracy on the results, guaranteeing the robustness of the modeling.

B. IEEE 14-Bus Test System

The modified IEEE 14-bus test system used in [3] has been selected to compare the presented approach with similar control algorithms available in the literature, namely the fast frequency response technique provided by a DFIG (proposed by Adu *et al.* [3]) and the virtual inertia technique of BESS of [21]. The three methods have been tested and compared by applying the same load event (i.e., connecting 50 MW at bus 13 at time $t = 1$ s). In the base case, a wind farm without any regulating capacity is injecting 36 MW at bus 2. Then, the plant has been substituted with the models available and able to provide inertia provision. All the parameters and settings given in [3] and in [21] have been replicated. In particular, in the first case, a wind plant with a DFIG machine with fast frequency response is assumed; in the

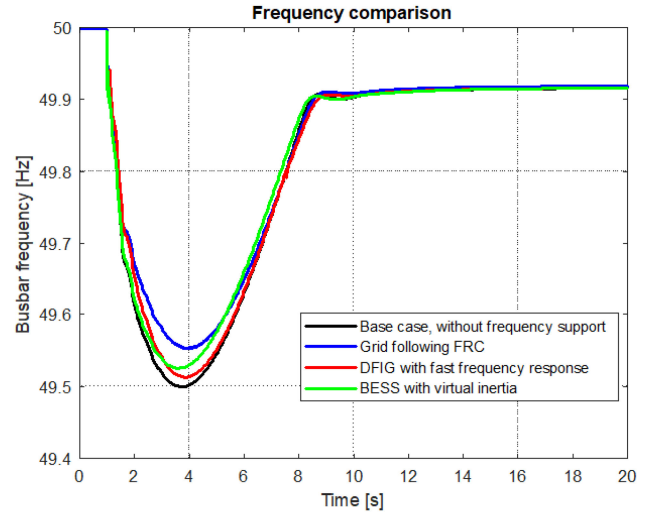


Fig. 16. Frequency comparison of the three approaches.

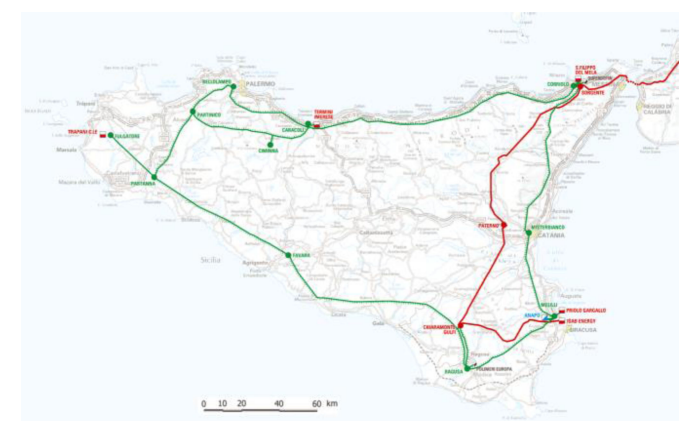


Fig. 17. HV grid considered.

second, a wind generator in parallel with a BESS of 45 MVA providing virtual inertia is considered, and in the third, a wind plant of 45 MVA with grid-following FRC equipped with the synthetic inertia control is tested. Here the dc-link capacitance has been adjusted according to (9).

Results are reported in Fig. 16: the base case in black is the system response provided by synchronous machines only; the red curve is the system behaviour with the DFIG fast frequency response [3], the green curve is given by the BESS according to [21], the blue one is the proposed approach. The figure shows that the proposed inertia emulation of the grid-following FRC presents the best results, both in terms of the lowest RoCoF and highest frequency nadir.

C. Simulation on the Real Transmission System

In this section, the proposed grid-following FRC control results are compared with the grid-forming approach on a portion of the Italian transmission network, the Sicilian grid (see Fig. 17) [22].

The Sicilian grid model adopted consists of about 540 HV busses (at 400, 230, 150, and 132 kV), 441 lines, more than

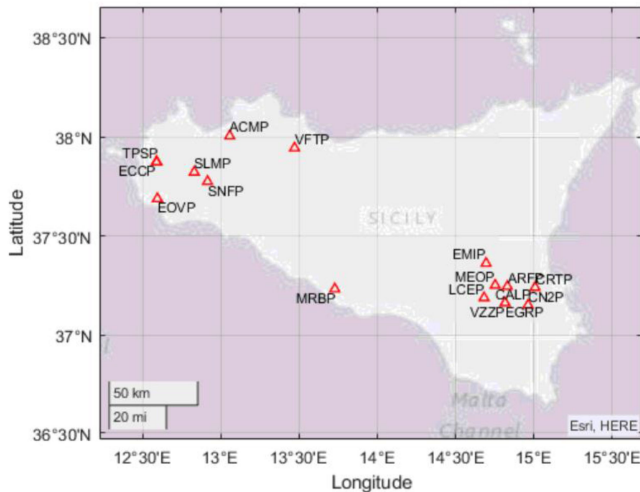


Fig. 18. Location of the wind farms in Sicily.

300 equivalent loads, 72 synchronous generators along with their frequency and voltage controllers, and 28 static generators, representing the largest PV and wind plants. The model also includes the actual governors and AVR of synchronous machines and the load shedding scheme implemented by the Italian transmission system operator, Terna. A total of 23 wind power plants are installed in Sicily, connected to the HV (132 and 150 kV) network through power converters, contributing to 4% of the total active power demand (2430 MW). Since 2016, Sicily is connected to the Italian system through two ac interconnections at 400 kV, both starting from Rizziconi substation in the mainland (Calabria) and getting to the Sorgente substation on the Island.

Each wind farm has been modeled and equipped with the proposed grid-following FRC control. The parameters of the control scheme introduced in Fig. 4 are assumed to be the same as in Table I, except for the nominal real power A_b that has been modified according to the real plants. The dc-link capacitance has been adjusted for each plant controller according to (9). Fig. 18 shows the location of the wind farms into the Sicilian grid.

During an import condition of approximately 220 MW from the continental system, Sicily disconnection has been used as a significant real power imbalance event, opening the connections with Calabria. The goal was also to employ the synthetic inertia to limit the frequency decay and avoid the load shedding scheme to be activated; its thresholds are set by Terna in its grid code, as recalled in [22], as follows.

- 1) From 49.3 to 49.1 Hz, based on RoCoF (from -0.3 to -1.2 Hz/s).
- 2) From 49.0 to 47.7 Hz based on pure frequency.

Fig. 19 directly compares the frequency responses with the inertial emulation of the proposed grid-following scheme, the grid-forming scheme and without emulation (base case). In the base case, only the synchronous machines provide the inertial response; the grid-forming case is obtained considering all wind farms to be equipped with VSM (grid-forming) converters,

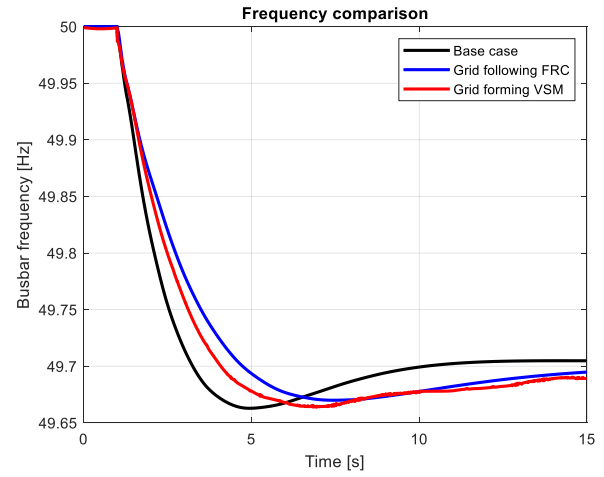


Fig. 19. Comparison of the frequency behavior with and without inertial response coming from the 23 wind turbine generators.

TABLE III
COMPARISON OF BASE CASE, GRID-FOLLOWING STRATEGY AND PROPOSED STRATEGY

Wind penetration is 4% of the total demand			
	Base Case	Grid-following FCR	Grid-forming VSM
Frequency	49.66 Hz @ 4.73 s	49.67 Hz @ 7.45 s	49.665 Hz @ 7.17 s
Initial RoCoF	-207.2 mHz/s	-110.3 mHz/s	-146.2 mHz/s

keeping the same operating conditions and perturbation. The mechanical time constant T_{VSM} has been set equal to 10 s. Fig. 19 shows that the approach proposed in this article, in blue, is the best in terms of both initial RoCoF and frequency nadir, thus making more unlikely the activation of the load-shedding scheme.

The tests made show that the emulated inertial response has a nonnegligible impact, resulting in a lower RoCoF and less probability of activation of the load shedding scheme. The results are given in Table III.

It is worth noticing that the proposed emulated inertia also positively impacts the normal operation of existing synchronous generation since generators ramp up and ramp down requirements are relaxed.

Additional analysis has been performed to validate the proposed grid-following approach assessing its robustness concerning different operating conditions. The wind penetration has been assumed to be higher (up to 182 MW, i.e., 7% of the load), keeping the same active power demand of 2430 MW. Sicily disconnection has been again used as a perturbation during an import condition of about 130 MW. Results are depicted in Fig. 20.

Once again, even in such new operating conditions, the inertial provision of the wind turbines effectively enhances the RoCoF and the frequency nadir, thus guaranteeing optimal security levels.

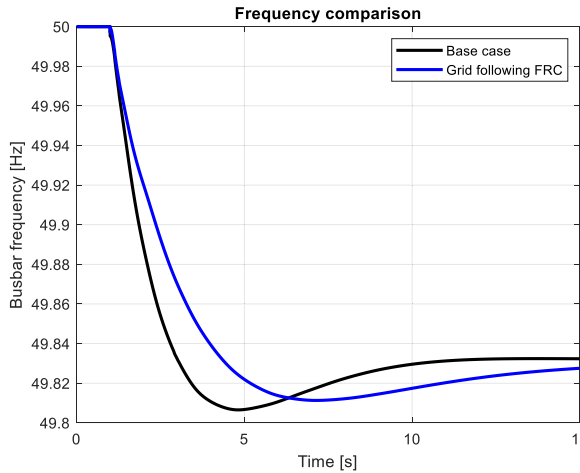


Fig. 20. Comparison of the frequency behavior with and without inertial response coming from the 23 wind turbine generators.

V. CONCLUSION

This article presents a strategy for the synthetic inertia provision from grid-following converters, either applicable to wind power, PV power, or storage systems. The proposed method can significantly improve power system stability against real power perturbations, thus giving the possibility of integrating large amounts of RES converter-based production in future power systems, keeping security at the usual highest standards.

The effectiveness of the proposed approach has been proved and compared to other strategies, namely grid-forming converters and controls of DFIG wind turbines, as well as BESS control, showing both better performances and a significant impact on the overall power system stability. Furthermore, given the current large spread of the grid-following converters, the approach can be easily applied to existing converters, with a slight change of the control logic, providing a sufficient energy buffer.

REFERENCES

- [1] A. Berizzi *et al.*, "Synthetic inertia from wind turbines for large system stability," in *Proc. IEEE Int. Conf. Environ. Electr. Eng. IEEE Ind. Commercial Power Syst. Eur.*, 2020, pp. 1–6, doi: [10.1109/EEEIC/ICPSEurope49358.2020.9160728](https://doi.org/10.1109/EEEIC/ICPSEurope49358.2020.9160728).
- [2] N. W. Miller and J. J. Sanchez-gasca, "Modeling of GE wind turbine-generators for grid studies," Apr. 16, 2010.
- [3] J. A. Adu, F. Napolitano, C. A. Nucci, J. Diego Rios Penalosa, and F. Tossani, "A DC-Link voltage control strategy for fast frequency response support," in *Proc. 20th IEEE Mediterranean Electrotech. Conf.*, 2020, pp. 470–475, doi: [10.1109/MELECON48756.2020.9140721](https://doi.org/10.1109/MELECON48756.2020.9140721).
- [4] M. F. M. Arani and E. F. El-Saadany, "Implementing virtual inertia in DFIG-based wind power generation," *IEEE Trans. Power Syst.*, vol. 28, no. 2, pp. 1373–1384, May 2013, doi: [10.1109/TPWRS.2012.2207972](https://doi.org/10.1109/TPWRS.2012.2207972).
- [5] X. Zhao, Y. Xue, and X.-P. Zhang, "Fast frequency support from wind turbine systems by arresting frequency nadir close to settling frequency," *IEEE Open Access J. Power Energy*, vol. 7, pp. 191–202, 2020, doi: [10.1109/oajpe.2020.2996949](https://doi.org/10.1109/oajpe.2020.2996949).
- [6] R. Jadeja, A. Ved, T. Trivedi, and G. Khanduja, "Control of power electronic converters in AC microgrid," *Power Syst.*, vol. 27, no. 11, pp. 329–355, 2020, doi: [10.1007/978-3-030-23723-3_13](https://doi.org/10.1007/978-3-030-23723-3_13).
- [7] U. Tamrakar, D. Shrestha, M. Maharjan, B. P. Bhattachari, T. M. Hansen, and R. Tonkoski, "Virtual inertia: Current trends and future directions," *Appl. Sci.*, vol. 7, no. 7, pp. 1–29, 2017, doi: [10.3390/app7070654](https://doi.org/10.3390/app7070654).
- [8] ENTSO-E, "Need for synthetic inertia (SI) for frequency regulation," Nov. 2, 2017.
- [9] D. Pattabiraman, R. H. Lasseter, and T. M. Jahns, "Comparison of grid following and grid forming control for a high inverter penetration power system," in *Proc. IEEE Power Energy Soc. Gen. Meet.*, 2018, pp. 3–7, doi: [10.1109/PESGM.2018.8586162](https://doi.org/10.1109/PESGM.2018.8586162).
- [10] R. H. Lasseter, Z. Chen, and D. Pattabiraman, "Grid-Forming inverters: A critical asset for the power grid," *IEEE J. Emerg. Sel. Top. Power Electron.*, vol. 8, no. 2, pp. 925–935, Jun. 2020, doi: [10.1109/JESTPE.2019.2959271](https://doi.org/10.1109/JESTPE.2019.2959271).
- [11] J. Zhu *et al.*, "Synthetic inertia control strategy for doubly fed induction generator wind turbine generators using lithium-ion supercapacitors," *IEEE Trans. Energy Convers.*, vol. 33, no. 2, pp. 773–783, Jun. 2018, doi: [10.1109/TEC.2017.2764089](https://doi.org/10.1109/TEC.2017.2764089).
- [12] M. Zhang, X. Yuan, and J. Hu, "Inertia and primary frequency provisions of PLL-Synchronized VSC HVDC when attached to islanded AC system," *IEEE Trans. Power Syst.*, vol. 33, no. 4, pp. 4179–4188, Jul. 2018, doi: [10.1109/TPWRS.2017.2780104](https://doi.org/10.1109/TPWRS.2017.2780104).
- [13] J. Fang, R. Zhang, H. Li, and Y. Tang, "Frequency Derivative-based inertia enhancement by grid-connected power converters with a frequency-locked-loop," *IEEE Trans. Smart Grid*, vol. 10, no. 5, pp. 4918–4927, Sep. 2019, doi: [10.1109/TSG.2018.2871085](https://doi.org/10.1109/TSG.2018.2871085).
- [14] A. Tayyebi, D. Groß, A. Anta, F. Kupzog, and F. Dörfler, "Interactions of grid-forming power converters and synchronous machines," Jun. 2019.
- [15] A. Bolzoni and R. Perini, "Feedback couplings evaluation on synthetic inertia provision for grid frequency support," *IEEE Trans. Energy Convers.*, vol. 36, no. 2, pp. 863–873, Jun. 2021, doi: [10.1109/TEC.2020.3021305](https://doi.org/10.1109/TEC.2020.3021305).
- [16] B. Wang, J. Ni, J. Geng, Y. Lu, and X. Dong, "Arc flash fault detection in wind farm collection feeders based on current waveform analysis," *J. Modern Power Syst. Clean Energy*, vol. 5, no. 2, pp. 211–219, 2017, doi: [10.1007/s40565-016-0233-4](https://doi.org/10.1007/s40565-016-0233-4).
- [17] A. Bolzoni and R. Perini, "Experimental validation of a novel angular estimator for synthetic inertia support under disturbed network conditions," in *Proc. 21st Eur. Conf. Power Electron. Appl. Eur.*, 2019, pp. 1–10, doi: [10.23919/EPE.2019.8914942](https://doi.org/10.23919/EPE.2019.8914942).
- [18] F. Luo, Y. M. Lai, K. H. Loo, C. K. Tse, and X. Ruan, "A generalized droop-control scheme for decentralized control of inverter-interfaced microgrids," in *Proc. IEEE Int. Symp. Circuits Syst.*, 2013, pp. 1320–1323, doi: [10.1109/ISCAS.2013.6572097](https://doi.org/10.1109/ISCAS.2013.6572097).
- [19] S. D'Arco and J. A. Suul, "Equivalence of virtual synchronous machines and frequency-droops for converter-based microgrids," *IEEE Trans. Smart Grid*, vol. 5, no. 1, pp. 394–395, Jan. 2014, doi: [10.1109/TSG.2013.2288000](https://doi.org/10.1109/TSG.2013.2288000).
- [20] I. Serban and C. P. Ion, "Microgrid control based on a grid-forming inverter operating as virtual synchronous generator with enhanced dynamic response capability," *Int. J. Electr. Power Energy Syst.*, vol. 89, pp. 94–105, 2017, doi: [10.1016/j.ijepes.2017.01.009](https://doi.org/10.1016/j.ijepes.2017.01.009).
- [21] J. A. Adu, J. D. Rios Penalosa, F. Napolitano, and F. Tossani, "Virtual in in a microgrid with renewable generation and a battery energy storage system in islanding transition," in *Proc. 1st Int. Conf. Energy Transit. Mediterranean Area*, 2019, pp. 1–5, doi: [10.1109/SyNERGY-MED.2019.8764108](https://doi.org/10.1109/SyNERGY-MED.2019.8764108).
- [22] D. Macallì, R. Zaottini, V. Illea, G. Giannuzzi, and A. Berizzi, "The role of load models and reactive power support during large frequency transients," in *Proc. 51st Int. Univ. Power Eng. Conf.*, 2016, pp. 1–6, doi: [10.1109/UPEC.2016.8114131](https://doi.org/10.1109/UPEC.2016.8114131).